



Full Length Article

Manufacture process and cabling optimization of Bi2212 CICC



Hang Zhao^{a,b}, Jinggang Qin^c, Lei Yu^{a,b}, Jianyuan Xu^{a,b}, Binglun Xiang^d, Hangwei Ding^a, Qingbin Hao^e, Pengcheng Huang^{a,*}, Wenge Chen^{a,*}

^a High Magnetic Field Laboratory, Hefei Institutes of Physical Science, Chinese Academy of Sciences, Hefei, Anhui 230031, China

^b University of Science and Technology of China, Hefei, Anhui 230026, China

^c Institute of Plasma Physics, Hefei Institutes of Physical Science, Chinese Academy of Sciences, Hefei, Anhui 230031, China

^d Baiyin Non-ferrous Changtong Wire & Cable Co., Ltd, Baiyin, Gansu 730900, China

^e Northwest Institute for Non-Ferrous Metal Research, Xi'an, Shanxi 710016, China

ARTICLE INFO

ABSTRACT

Keywords:

Bi2212 superconducting cable
CICC
Manufacture process
Cabling optimization
HTS

The Bi2212 cable-in-conduit conductor (CICC) is a composite soft material and is sensitive to stress-strain and brittle breakage. The cabling tensions are critical parameters for the CICCs and have undergone trial production many times to achieve effective cable control. Unreasonable tension will cause circumferential and axial motion, resulting in deflection bending, rotation fluctuations, and wire slip. This study investigated the manufacturing process of the Bi2212 CICC, optimizing the cable twisting process and reducing manufacturing consumption and damage. Additionally, optimized tensions of the Bi2212 CICCs during the cabling process, focusing on pay-off tension, rotation speeds, and traction tensions were presented. Finally, the results are tested and verified in the factory to examine the wire jumpers, serpentine bending, and pitch fluctuations. This research provides useful references for future cable fabrication of the HTS CICCs.

1. Introduction

The hybrid magnet, characterized by a strong magnetic field, facilitates extreme experimental conditions for material properties [1]. Following the development of the 40 T and 45.22 T hybrid magnets [2, 3], the High Magnetic Field Laboratory of China (CHMFL) is focused on a 55 T hybrid magnet. The conceptual design includes an SC outsert magnet providing a central magnetic field of 20 T. The contribution of the Bi2212 coil is 10 T@ 20.8 T in conceptual design, the cold aperture diameter is 920 mm, and the operating temperature is 4.5~5.0 K. The expected higher field requires promising high-temperature superconducting (HTS) CICCs, and their performance determines the stability of the hybrid magnet.

Bi2212 superconductor has a high H_{c2} up to 100T at 4.2 K, and round wire offers isotropic and excellent current-carrying performance at high fields, making it a promising candidate for the 55 T hybrid magnet [4,5]. Research shows that the Bi2212 cable is made into the CICC type and proves excellent performance above 20 K with a 10 kA @ 12 T [6]. Then, the Bi2212 cable is applied in hybrid magnets with Nb₃Sn, using a heat-in-tube method up to 50~60 bar and supercritical helium through the center tube [7]. Currently, kilometer-length Bi2212 wires with high

current density (J_e) for high-field applications can be produced at the NIN institute [8,9]. Pre-overpressure heat treatment process has been proven to prevent strand loosening and enhance critical performance [10,11]. In 2017, the Chinese Academy of Sciences (CAS) manufactured a Bi2212 CICC with 13.1 kA @ 4.2 K using a pure-Ag tube [12]. Despite advancements in the manufacturing process, wire enhancement, and heat treatment for the Bi2212 CICC, mechanical research remains less explored.

The Bi2212 wire relies on multifilament, Ag-coated, and composite soft material. The mechanical properties are a critical issue due to its brittleness and sensitivity to stress-strain in CICC development [13,14]. The applied tension and uniformity have a direct impact on the cable damage and superconductivity. Unreasonable cabling force, bending deformation, or contact indentation [15] will cause sheath rupture and SC powder leakage [16], as observed in both the Rutherford [17] cable and CICCs. As is known, in the ITER project, cabling tensions are vital parameters for TF&PF CICCs, and multiple trial productions have been undertaken to achieve effective tension control [18,19].

However, the cabling force of the Bi2212 CICC in recent studies is tensionless due to the wire damage, which cannot be estimated [12]. The degradation mechanism indicates that the Bi2212 CICC becomes

* Corresponding authors.

E-mail addresses: hpc@hmfl.ac.cn (P. Huang), wgchen@ipp.ac.cn (W. Chen).

unstable when the void fraction increases to 35–40 % due to lower tensions [20]. This instability can cause uneven pitch, shape deformation, porosity fluctuation, and wire slip, severely impacting the future performance of the hybrid magnet. Research has proved that unreacted wires can retain more than 95 % critical current (I_c) when the indentation is within 26 % of the diameter [21], which provides a reference for radial indentation during cabling. However, the effects of axial tension during cabling have not been addressed.

Therefore, optimized tension is needed to ensure the cable is compact, uniform in structure, and stable in twist pitch. Stress management concepts must be applied to Bi2212 CICC to achieve better performance of the 55T hybrid magnet. This study investigated the mechanical properties of the Bi2212 CICC during the cabling process. The analysis focused on optimizing the tension range for cable twisting, including pay-off tension, traction tension, and rotation speed for practical applications. This research provides useful references for designing and manufacturing the HTS CICCs with optimized mechanical parameters.

2. Bi2212 wire specifications and CICC model

The Bi2212 round wire is composed of specific silver content, Ag alloys, and Bi2212 filaments. The CICC is made up of hundreds of Bi2212 wires twisted together with different configurations. Therefore, the wire specifications are the basic input parameters of the CICCs.

Fig. 1 presents the tensile test of the Bi2212 wire at 300 K, and shows that the slope of the curve changes significantly near the 0.1 % point. In fact, the Ag or Ag-Alloy has yielded and elongated in the initial elastic stage over 45 MPa, the nonlinear elastic relationship mainly results from the superposition of stress and strain of each component in the material. Research in the evolution of Young's modulus with the strain has proved that the slope of the initial elastic domain approximates linear. The initial elastic modulus approaches the limit of the linear part of the unloading path [22]. During the twisting process of CICC cables, significant wire strain is not allowed, so the allowable tension should be around 0.1 % of the strain during cabling at 300 K. Therefore, the allowable yield point of the Bi2212 wire can be set to 45 MPa, instead of the maximum breaking stress to prevent damages. The input parameters are shown in Table 1.

The hybrid magnet adopts a four-stage configuration of the Bi2212 CICC to provide about 18.5 kA. Four-stage cables can be more compact, uniform in heat treatment at 895°C, and easier to manufacture. Dummy conductors were arranged in a $3 \times 4 \times 5 \times 6$ configuration with various

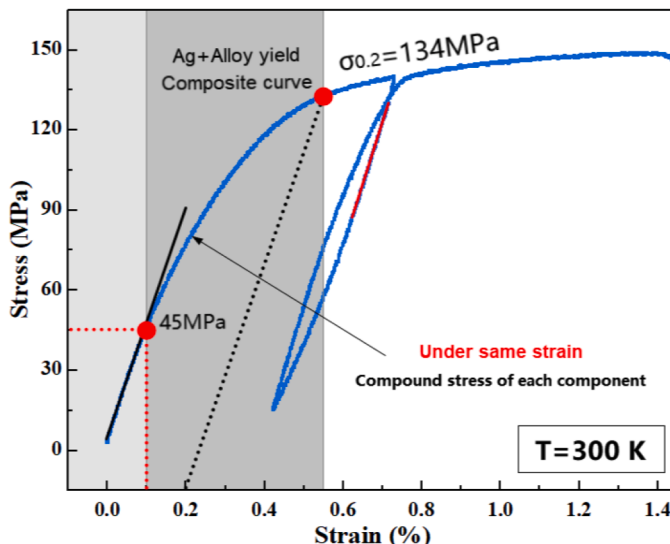


Fig. 1. Tensile test and analysis of the Bi2212 wire.

Table 1

Input parameters of Bi2212 superconducting wire.

Items	Value	Items	Value
Filament/bundle	55 × 18	Max strain (%)	0.47 %
Size (mm)	$\Phi 1.0 \pm 0.02$	Bi2212 ratio (%)	25.29
I_c (A)	$\geq 400 @ 12T$	Ag and alloy (%)	74.71
E (GPa)	50.2	Density (kg/m ³)	9800
YS (MPa)	134	UTS (MPa)	155

spiral angles and patterns.

3. Manufacture process

Since the helical type of the CICC is complex in its three-dimensional structure, it is practically difficult to describe the mechanical behavior during the cabling process. However, the Bi2212 CICC cable has different strength and wire specifications from the NbTi and Nb₃Sn CICCs, as shown in Table 2. Due to the high silver content of 74 % of Bi2212 superconductor, it is inferior to traditional CICCs in the cabling tension and manufacturing process. Unreasonable cabling force will cause circumferential and axial motion, resulting in deflection, rotation fluctuations, and wire slip.

To a large extent, the manufacturing process of the CICC cable strands is affected by friction coefficient, cabling tensions, rotation speed, twist pitch, cable diameter, and cable configuration. Table 3 presents the cable diameters and helical radius [23]. The subcables of each stage should be arranged symmetrically during the cabling process. The symmetry and uniform force distribution of each subcable will make the cable pitch more stable. Bi2212 wire has low yield strength and is sensitive to stress. Uneven concentrated stress will be generated during the initial start-up of the equipment, and the machine should be started slowly, accelerated gradually, and the process should be as smooth as possible.

Due to the high friction coefficient of the pure silver sheath, Bi2212 is very prone to tensile fracture during rotation and stretching. The friction coefficient of the Bi2212 wire is 3~4 times more than the NbTi and Nb₃Sn with Cu-sheath. To reduce the friction, the original steel pulleys of the winch were replaced with smooth nylon pulleys, and 10 to 20 mm polytetrafluoroethylene (PTFE) tape was wrapped around. The cable bobbin and pay-off plates were wiped clean with organic solvents. T-type PTFE bushings with smoothed round corners are installed along the winch. The layout of the winch is shown in Fig. 2.

Fig. 3 depicts the partial view of the sub-cable before entering the compact die during the manufacturing process. Considering excessive friction, vibration, and start-up, the practical distance between the cable distributor and the compact die should be lower than the theoretical results. Due to its high friction coefficient and long stress release time, the Bi2212 is not suitable for shorter distances. This study recommends a distance of 250 mm or more ($\alpha \leq 2\beta$) as an empirical range. Reducing the distance will increase the α before entering the compact die, which is unfavorable for Bi2212 cable strands. The rotation speed in Stages I and II should be controlled within 1 r/s (6.28 rad/s).

Table 2

Superconducting wire specifications.

Material	State	Diameter (mm)	T(K)	E GPa	YS MPa	UTS MPa
Bi2212	Unreacted	1.0	300K	45.3	172	201
	reacted	0.96	4.2K	127	161	248
Nb ₃ Sn	Unreacted	0.82	300K	61	196	582
	reacted	0.82	4.2K	173	248	310
NbTi	/	0.73	300K	60	295	643
			4.2K	151	270	1073

Note: The Nb₃Sn data is from the test of CHMFL, and the NbTi data is from the test data in [24].

Table 3Cable radius of the CICC cable (pattern: $3 \times 4 \times 5 \times 6$).

Material	Items	Radius	1st-stage	2nd-stage	3rd-stage	4th-stage
Bi2212	outer radius	0.50/0.48	1.08	2.32	5.57	16.70
	spiral radius	0	0.58	1.24	3.25	11.13
Nb ₃ Sn	outer radius	0.41	0.88	1.90	4.56	13.69
	spiral radius	0	0.47	1.02	2.66	9.13
NbTi	outer radius	0.365	0.79	1.69	4.06	12.19
	spiral radius	0	0.42	0.91	2.37	8.13

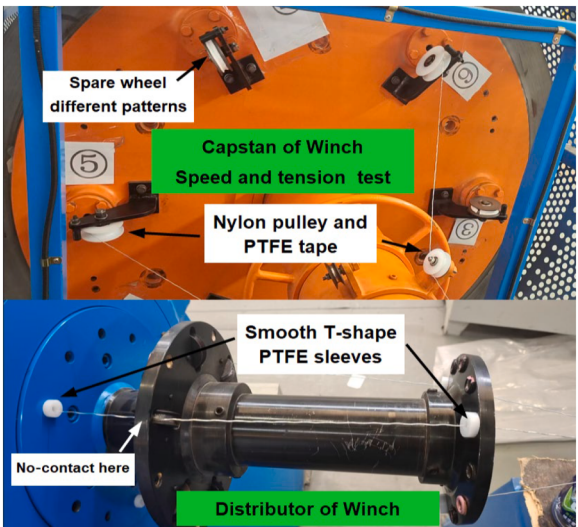


Fig. 2. Improvement and overall layout of cable winch.

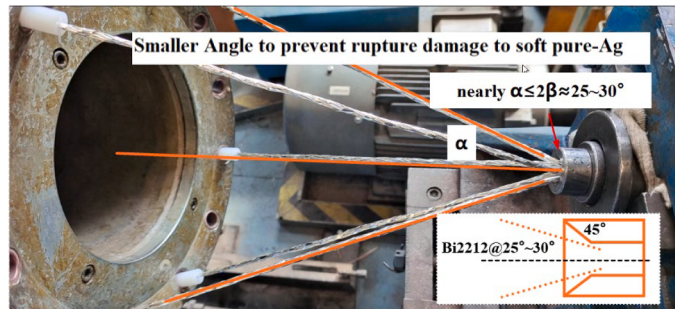


Fig. 3. Test and analysis of compact process for Bi2212 cables.

4. Cabling tension optimization

The CICC cable strands are all twisted right-handed from the primary subcable to the final stage and are easy to loose. Different wire materials have various tension requirements. Low-tension cabling process will cause circumferential and axial motion of the wires or sub-strands, leading to fluctuations in length, twist pitches, and spiral radius from the central axis [25]. The fluctuations can easily result in serpentine bending, which is the main factor causing the cable deformation. On the contrary, excessive pay-off tension will also result in the strands becoming overly tight, preventing the internal stress from being fully released before entering the compact die. The residual stress will lead to

cable bending, uneven distribution, and surface rupture [26]. Therefore, improper cabling tension can lead to performance degradation and even operational risks, which need to be optimized.

Fig. 4 depicts the 3D model of the twisting process. Technical parameters during the cabling process, including pay-off tension, rotation speed, and traction tension, will be optimized and tested. The diameter of the large distributor plate is 175 mm, the small distributor plate is 110 mm, and their distance measures 300 mm. The angle β is fixed at $\pi/30$, and the angle α can be adjusted, ranging from 180 mm to 300 mm. The greater the distance, the smaller the alpha, and is easier to pass through the compact-die. However, a larger distance will increase the deflection between the two points and will reduce the stability of the sub-strands. Especially for Ag-sheath SC wires with high friction, a greater distance will reduce scratching and indentation when passing through the compact dies.

4.1. Deflection effect

The CICC factory has three sets of winches for manufacturing the Bi2212 cables. The distance from the cable distributor to the compact die can be adjusted from 170 mm to 400 mm. In the study, the distance was set to 350 mm. Fig. 5 illustrates the mechanical analysis of deflection during the cabling process. Eqs. (1–3) demonstrate the correlation between the deflection y and the tension T at both ends [27].

$$y = -ch\left(\frac{Wx}{H} + C\right) \frac{H}{W} + D \quad (1)$$

$$T_x = H \cdot ch\left(\frac{Wx}{H} + C\right) \quad (2)$$

C and D represent the integral constants in the equation, as shown below.

$$C = sh^{-1}\left(\frac{WL}{H \cdot sh(-WL/H)}\right) \quad D = \frac{ch(-WL/H + C)}{shC \cdot sh(-WL/H)} \quad (3)$$

where H represents the horizontal component of tension, W denotes the line weight of the cable, L is the horizontal distance from the cable distributor to the compact die, and T signifies the tension at both ends.

Due to the large size of high-level subcables, the line weight of the 2nd and 3rd stages increases significantly, and higher tensions will be required at both ends to prevent cable deflection. Figs. 6 and 7 depict the deflection variation with pulling tensions. They exhibit a quadratic relationship, and the deflection gradually stabilizes as the tension increases. The minimum tension is approximately proportional to the square of the distance between the cable distributor and the compact die. Doubling the distance results in a rapid four-fold increase in the minimum tension. A minimum tension exists that causes minimal deformation and fluctuation of the CICC cable strands, which can be calculated and listed in Table 4. The corresponding tensile forces are 14.5 N, 25.0 N, 80.0 N, and 186.8 N from single wire to stage IV. Hence, wire deformation and serpentine bending caused by deflection can be eliminated under these tensions.

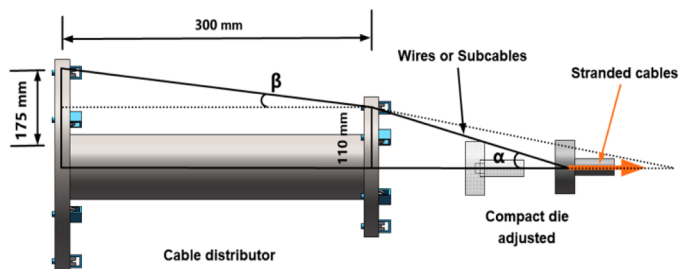


Fig. 4. The 3D model from cable distributor to compact die.

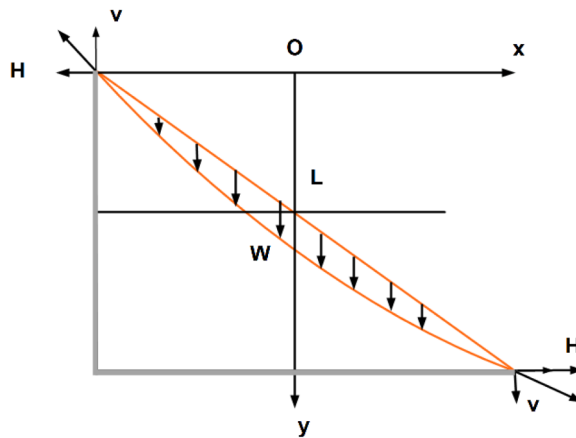


Fig. 5. Mechanical analysis of deflection in Bi2212 CICC strands.

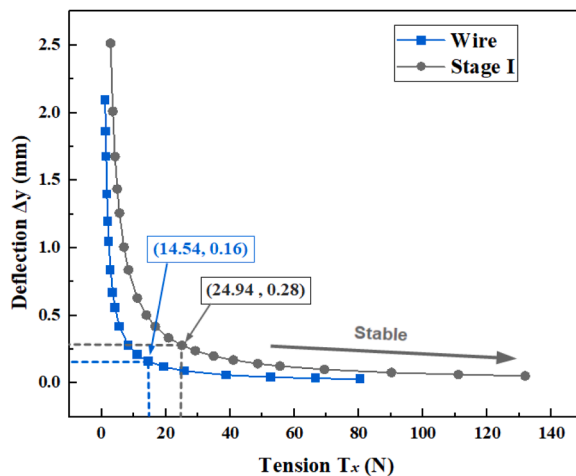


Fig. 6. Deflection vs. tension of the wire and primary stage.

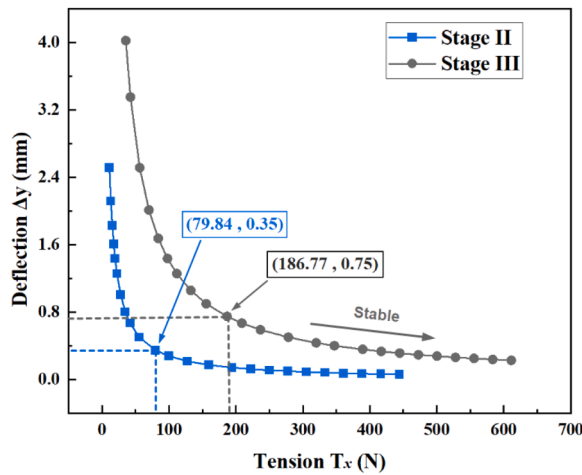


Fig. 7. Deflection vs. tension of stages II and III.

Fig. 8 depicts that the tension increases significantly as the distance increases. Stage I requires greater tensile force than the primary single wires due to the increased line weight. The tension at a deflection of 0.1 mm increases from 22.8 N to 69.7 N When the distance increases from 200 mm to 350 mm. The wire increases from 7.6 N to 23.2 N, nearly threefold. Considering different deflections with a distance of 350 mm,

Table 4

The deflection vs. tension of Bi2212 CICC strands.

	Helical radius	Strand weight W (kg/m)	Mid-deflection Δy (mm)	Tension T_d (N)
Wire→stage I	0.000	0.0077	0.16	14.54
stage I→II	0.577	0.0232	0.28	24.94
stage II→III	1.241	0.0928	0.35	79.84
stage III→IV	3.246	0.4643	0.75	186.77

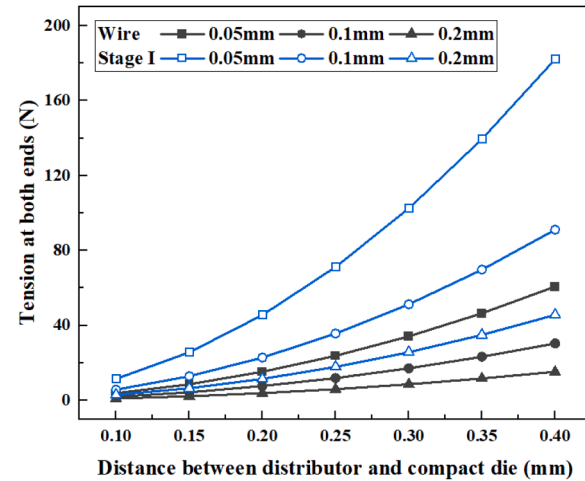


Fig. 8. Tension vs. distance of wire and stage-I.

the tensile force at 0.05 mm deflection is nearly four times that at 0.2 mm deflection.

Bi2212 superconductors have lower yield strength and a soft pure-Ag sheath. The initial distance should be as large as possible with a lower α to reduce indentation and rupture. However, reducing the distance is beneficial for minimizing tensile forces while the tension exceeds the allowable stress. Therefore, an optimized distance can be obtained.

4.2. Rotation effect

Improper centrifugal force will lead to fluctuations in tension due to the rotational inertia force. Traditionally, winch rotating at a lower speed is preferred to prevent deformation of the superconducting CICC cables. However, a lower rotation speed will waste more time and affect manufacturing efficiency significantly, especially in stages I and II. The faster the rotation speed, the greater the tension required. Thus, the minimum tension and appropriate speed range for the Bi2212 CICCs need to be determined.

In Fig. 9, the F_c represents the centrifugal force, L denotes the total length of the cable, T denotes the tension at both ends, R represents the

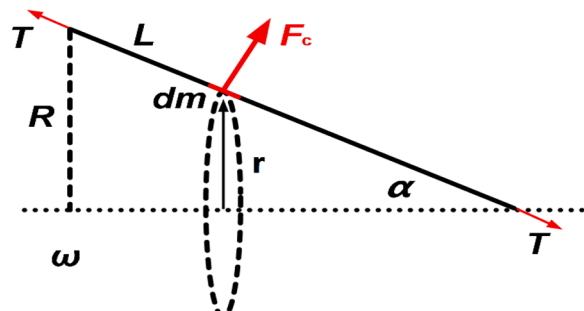


Fig. 9. Mechanical analysis of Bi2212 CICC cable during rotation.

cable distributor radius, ω is the rotational speed, and d_m is the micro-element of mass.

Using the rotational inertia force equation, $F = m\omega^2 r$, a differential equation can be derived:

$$dF = r\omega^2 \cdot dm = l \sin\alpha \cdot \omega^2 \cdot \rho \cdot dl \quad (4)$$

The cable depicted in Fig. 8 can be integrated along the length L to determine the centrifugal force F_c acting on the cable using the Eq. (5).

$$F_c = \int_0^L \rho \omega^2 \sin\alpha \cdot l \, dl \quad (5)$$

In this study, the speed is set at 2π rad/s. The distributor radius is 175 mm, and the distance is 350 mm. The maximum centrifugal force of cable bending will be concentrated at the maximum deflection point, where the force acts vertically on the cable in Fig. 9. The tension at both ends can offset the centrifugal deformation and bending fluctuations. However, the tension should not exceed the allowable stress of the Bi2212 cable. Combined with Eq. (6), the tension at both ends required is shown in Table 5.

The rotation speed of the CICC cable strands is generally controlled at $0.5\sim2$ r/s ($3.14\sim12.56$ rad/s). Fig. 10 shows the tension with different rotation speeds of the capstan. The minimum tension is proportional to the square of the rotational speed. Doubling the rotational speed leads to a four-fold increase in the inertia force. The wire and stage I with lower line weight experience smaller centrifugal force than the higher stages when the capstan rotates, keeping the tension below 30 N, which has a slight impact on tensions. However, the tension in high-stage cables at stages III and IV increases rapidly when the rotation speed exceeds 3 rad/s. In practical applications, higher stages must eliminate the influence of rotation on the tensions. To maintain the tension below 60 N, the rotation speed must be controlled below 7.9 rad/s and 5.3 rad/s, respectively.

4.3. Traction force

The traction tension is higher than the pay-off tension due to friction and tensile resistance in practical applications. The traction force of the take-up pulley behind the compact die is primarily influenced by factors such as failure stress, cable diameter, traction pulley, pay-off tension, and friction. The traction force should not be higher than the allowable tension determined by the yield strength. Therefore, the traction tension and speed of the take-up pulley should be selected to ensure that the sub-strands remain within the maximum limit. The tension of CICC strands can be represented:

$$\sigma = \frac{T_t}{\pi/4 \times n \times d^2} \quad (6)$$

The Eq. (6) assumes that the wire lies parallel to each other. However, the structure of each cable is spiral, with the internal wires subjected to higher tension than parallel wires. The strands around the take-up pulleys will experience additional bending stresses, which can be obtained by Rouleaux's equation as follows [28].

$$\sigma = \frac{T_t}{\pi/4 \times n \times d^2} + \frac{d}{D} \times E \quad (7)$$

Table 5

The relationship between the tension and the rotation speed during twisting of the Bi2212 cable.

	R / L_0 (mm)	ρ_L (kg/m)	$\pi/2\theta$ (rad)	Deflection (mm)	T (N)
Wire→stage I	175/350	0.0077	1.5700	0.16	6.40
stage I→II	175/350	0.0232	1.5694	0.28	10.96
stage II→III	175/350	0.0928	1.5690	0.35	35.07
stage III→IV	175/350	0.4643	1.5670	0.75	81.86

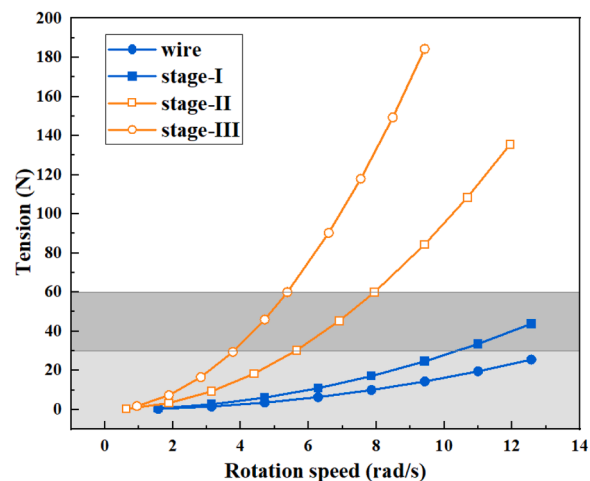


Fig. 10. Tension vs. rotation speeds of the capstan.

Therefore, the modulus E should be selected from the equivalent cable modulus of each stage rather than the single SC wires. The maximum traction force T_t can be obtained from Eq. (7), and the results are shown in Table 6. Moreover, safety factors will be adjusted from the practical cabling experiments to ensure reliability during operation.

The maximum traction force progressively increases with the growth of the cable pattern. The diameter of the traction wheel in the CICC winches is much larger than the diameter of the wire, so the diameter of the traction wheel has little effect on the maximum traction force. However, the allowable strength and equivalent elastic modulus at each sub-stage have a great contribution to the traction force results.

4.4. Cabling tension test and optimization

In practical applications, the pay-off tension resists flexural and centrifugal forces to prevent the cables from being loose, serpentine deformation, and twist pitch deviations. The total force can be represented as $T_p = T_d + T_r$. The maximum allowable traction force increases with wire diameter and the equivalent elastic modulus. Traction speed and force are related to the rotation of the capstan, generating a centrifugal force and increasing the tension at both ends.

The special characteristics of the Bi2212 wire make it more sensitive to stress and strain, and the stress above 45 MPa may lead to irreversible tensile deformation of the wire, according to Fig. 1. The cabling tension must be reduced as much as possible to retain sufficient safety margin. The tensile strain of Stage I to IV cables will ultimately be converted into the strain of the internal wire itself. This paper takes 50/90/140/190 mm to obtain the strain of each sub-cable from stage I to IV. As shown in Fig. 11, the cable with a four-stage contains 1.007 m of SC wire per meter when the axial strain of stage IV is 0.1 %. The corresponding strain of the internal wire is 0.0993 %. The study found that the strain of the internal wire is slightly smaller than the strain of the cable itself, and their deviation is less than one hundred thousandths.

Therefore, the cable strain at each stage in the cabling process is calculated at a maximum value of 0.1 % to prevent excessive damage to the Bi2212 strands.

Table 6

Maximum traction force of Bi2212 CICC strands.

	Allowable stress (MPa)	Safety factor	D (mm)	E (GPa)	T_t (N)
Stage I	28.805	0.90	1250	32.13	34.86
Stage II	24.546	0.85	1250	27.38	154.04
Stage III	20.518	0.80	1250	22.89	833.55
Stage IV	10.898	0.75	1250	12.16	6792.74

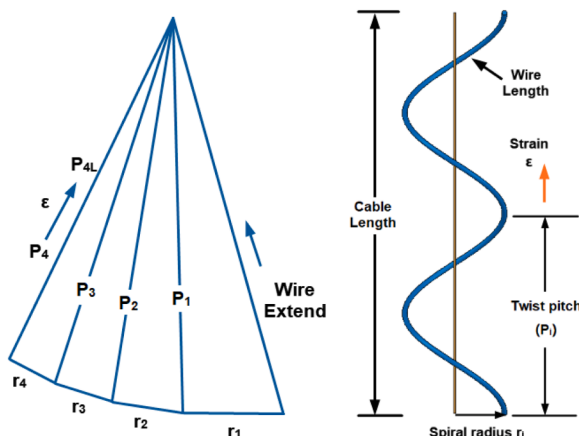


Fig. 11. Tensile strain between stage IV and internal wires.

However, the different twist pitches of the CICC cables will affect the cable helix radius and twisting coefficient, resulting in changes in the wire diameter and weight W , as shown in Eqs. (1) to (3). The maximum tension at both ends will also increase with the twist pitch and wire number in stage I, stage II, and stage III cables. Therefore, the variation of twisted pitch can lead to fluctuations in deflection and centrifugal force and the long twist pitch can withstand higher tensile strength, which can maintain high tensile strain in the axial direction. However, the internal wires of long twist pitch cables will bear greater wire stress, the practical tension during the cabling process will be much lower than the maximum tension limit, and the minimum cabling tension is the main point to determine the cable's serpentine bending, pitch fluctuations, and uniform distribution. So the optimized tension should be appropriately reduced compared to the theoretical value rather than the maximum strength. The soft Ag-sheath determines the tension range in this study and is sufficient to eliminate the negative effects of tensionless in the Bi2212 cabling process rather than the yield point of the Bi2212 filaments to prevent cable damage.

The optimized pay-off tensions (T_p) and traction tensions (T_t) of each stage are shown in Table 7. Generally, the CICC strands over three stages contain dozens to hundreds of wires, and the internal stress and structure are unevenly distributed due to factors such as friction, vibration, and start-stop. Once some of the strands are broken, the stress of the remaining SC wires will rise suddenly. Therefore, a certain safety margin needs to be considered with allowable tension within 0.1 % of the cable strain.

The cabling tension was tested at the CICC factory to monitor the surface damage and assess the reliability of the calculation results. To ensure the accuracy of the test, a new cable winch without mechanical wear and a calibrated tension controller were installed with high stability. The designed cable tension range is tested, and the comparison between the optimized and tested tension is shown in Table 8. Research finds the test results in stage I are higher than the theoretical range, and the main reason is that the tension of the primary cable is relatively small, and it is more sensitive to fluctuation and resistance. The stages II

Table 8
Test and verify the reliability of the optimized tensions.

Items	Pay-off tension(N)		Traction tension(N)	
	Optimal range	Test range	Optimal range	Test range
Stage I	15~25	20~35	20~30	25~45+
Stage II	45~65	40~75	100~150	120~200+
Stage III	130~150	100~200+	400~600	400~600+
Stage IV	300~400	250~450+		

The cable performed well in the test range, no obvious fluctuations.

and III sub-cables are more consistent with the test results.

To verify the traction tension, a counterweight was added to the cable, and the cable was manually measured and recorded. The test results showed that the elongation did not exceed 1 % of the total length (5 m). No obvious jumpers, serpentine bending, stress release rotation, or uneven pitch distributions were observed by visible examination. The test region of the pay-off tension is wider than the optimized values. Twisted cables with tensionless and optimized tension are shown in Fig. 12. The tested tension did not reach the critical value to avoid affecting the subsequent manufacturing process. The test has shown that the theoretical range is reasonable and has a certain margin for practical applications.

5. Discussion and conclusions

This study investigates the manufacturing process of the Bi2212 CICC cable, optimizing the cable twisting process to improve the stability of the twisting process and reduce manufacturing consumption and damage. Moreover, the mechanical properties, such as pay-off tension and traction tension, during the cabling process of the Bi2212 CICC were analyzed and optimized.

Firstly, the cable deflection and capstan rotation were analyzed to determine the minimum tension of each sub-cable to prevent serpentine bending, fluctuation, or excessive twisting. The deflection exhibits a quadratic relationship with the cabling tensions and gradually stabilizes as the tension increases. The minimum tension is approximately proportional to the square of the distance between the cable distributor and the compact die.

In addition, the maximum tractive force of the cable has been proposed to ensure safety and reliability during operation. The rotational speeds and the diameter of the traction wheel have little effect on the traction force. However, the number of wires and cable configurations will affect the effective elastic modulus and diameter, which have a



Fig. 12. Twisted cables with tensionless and optimized tension.

Table 7
Practical tension range for Bi2212 cabling process.

Items	Stage I	Stage II	Stage III	Stage IV
Wire number	3	12	60	360
Equivalent modulus (GPa)	32.13	27.38	22.89	12.16
Safety factor	0.90	0.85	0.80	0.75
Allowable tension(N)	105.45	416.18	1892.6	7982.5
Min pay-off tension(N)	20.93	35.90	114.91	268.63
Max traction tension(N)	34.86	154.04	833.55	6792.74
Optimized tension T_p (N)	15~25	45~65	130~150	300~400
Optimized tension T_t (N)	20~30	100~150	400~600	1500~2500

great contribution to the traction force. The calculation method was presented.

Finally, the practical tension range for the Bi2212 CICC strands was obtained from the allowable tension, minimum pay-off tension, and maximum traction tensions. The tension range was tested at the CICC factory to assess the reliability of the theoretical results. No obvious jumpers, serpentine bending, stress release rotation, or uneven pitch distributions were observed by visible examination. The test results have shown that the design range is reasonable and has a certain margin for practical applications.

CRediT authorship contribution statement

Hang Zhao: Writing – original draft, Software, Methodology, Investigation, Conceptualization. **Jinggang Qin:** Project administration, Funding acquisition. **Lei Yu:** Visualization, Formal analysis, Data curation. **Jianyuan Xu:** Validation, Formal analysis. **Binglun Xiang:** Validation, Supervision. **Hangwei Ding:** Supervision, Formal analysis. **Qingbin Hao:** Supervision, Resources. **Pengcheng Huang:** Writing – review & editing, Supervision. **Wenge Chen:** Writing – review & editing, Supervision, Project administration.

Declaration of competing interest

The authors declare that they have no known competing financial interests or personal relationships that could have appeared to influence the work reported in this paper.

Data availability

The data that has been used is confidential.

Acknowledgements

The authors would like to acknowledge the support from the National Natural Science Foundation of China (Grant No. U2032216) and the Key Program of Research and Development of Hefei Science Center, CAS (Grant No.2019HSC-KPRD002). The author appreciates the support from the Baiyin Non-ferrous Innovation Co., Ltd for the assistance in the mechanical testing.

References

- [1] Mitsuhiro Motokawa, Physics in high magnetic fields, *Rep. Prog. Phys.* 67 (11) (2004) 1995–2052, <https://doi.org/10.1088/0034-4885/67/11/R02>.
- [2] W.G. Chen, Z.M. Chen, Z.Y. Chen, et al., Development of the heat treatment system for the 40 T hybrid magnet superconducting outsert, *J. Sci. Instrum.* 82 (2011) 105106, <https://doi.org/10.1063/1.3652978>.
- [3] Z. Fang, W.G. Chen, P.C. Huang, et al., Test operations of the upgraded hybrid magnet at CHMFL, *IEEE Trans. Appl. Supercond.* 34 (5) (2024) 4300705, <https://doi.org/10.1109/TASC.2024.3350581>.
- [4] D.C. Larbalestier, J. Jiang, U.P. Trociewitz, et al., Isotropic roundwire multifilament cuprate superconductor for generation of magnetic fields above 30T, *Nat. Mater.* 13 (2014) 81–88, <https://doi.org/10.1038/nmat3887>.
- [5] J. Jiang, G. Bradford, S.I. Hossain, et al., High-performanceBi-2212 round wires made with recent powders, *IEEE Trans. Appl. Supercond.* 29 (2019) 6400405, <https://doi.org/10.1109/TASC.2019.2895197>.
- [6] T. Isono, Y. Nunoya, T. Ando, et al., Development of 10 kA Bi2212 conductor for fusion application, *IEEE Trans. Appl. Supercond.* 13 (2) (2003) 1512–1515, <https://doi.org/10.1109/TASC.2003.812763>.
- [7] J. Breitschopf, D. Chavez, T. Elliott, et al., 2-layer Cable-in-Conduit for Hybrid-Coil Magnets, in: IOP Conf. Series: Materials Science and Engineering 756, 2020 012031, <https://doi.org/10.1088/1757-899X/756/1/012031>.
- [8] S.N. Zhang, X.B. Ma, L.J. Cui, et al., Fabrication and optimization of Bi-2212 high temperature superconductors with K and Ag co-incorporation, *J Mater Sci-Mater El* 30 (2019) 3418–3425, <https://doi.org/10.1007/s10854-018-00616-y>.
- [9] B. Yang, Q.B. Hao, P. Xiao, et al., Preparation of high-performance high temperature superconducting Bi-2212 wires by the spray pyrolysis powder, *J. Mater. Sci. Mater. Electron.* 34 (2023) 1681, <https://doi.org/10.1007/s10854-023-11072-8>.
- [10] P. Chen, *Processing and Characterization of Superconducting Solenoids Made of Bi-2212/Ag-alloy multifilament Round Wire For High-Field Magnet Applications [D]*, Florida State University, 2016.
- [11] D.S. Yang, M. Yu, H. Ma, et al., Performance of first Bi-2212 cable with pre-over pressure and overpressure heat treatment, *Supercond. Sci. Technol.* 35 (1) (2022) 015007, <https://doi.org/10.1088/1361-6668/ac30ea>.
- [12] J.G. Qin, Y. Wu, J.G. Li, et al., Manufacture and Test of Bi-2212 cable-in-conduit conductor, *IEEE Trans. Appl. Supercond.* 27 (99) (2017) 1–5, <https://doi.org/10.1109/TASC.2017.2652306>.
- [13] M. Brown, E. Bosque, D. McRae, Tensile properties and critical current strain limits of reinforced Bi-2212 conductors for high field magnets, *IOP Conf. Series: Mater. Sci. Eng.* 279 (2017) 012022, <https://doi.org/10.1088/1757-899X/279/1/012022>.
- [14] C. Dai, J.G. Qin, B. Liu, et al., Uniaxial strain induced critical current degradation of Ag-sheathed Bi-2212 round wire, *IEEE Trans. Appl. Supercond.* 28 (3) (2018), <https://doi.org/10.1109/TASC.2017.2787133>.
- [15] J.G. Qin, C. Dai, Q.L. Wang, Impact of indentation on the critical current of bi2212 round wire, *IEEE Trans. Appl. Supercond.* 26 (4) (2016) 8401005, <https://doi.org/10.1109/TASC.2016.2532324>.
- [16] K. Zhang, H. Higley, L.Y. Ye, Tripled critical current in racetrack coils made of Bi-2212 Rutherford cables with overpressure processing and leakage control, *Supercond. Sci. Technol.* 31 (2017) 105009, <https://doi.org/10.1088/1361-6668/aada2f>.
- [17] T.M. Shen, L.G. Fajardo, Superconducting Accelerator Magnets Based on High-Temperature Superconducting Bi-2212 Round Wires, *Instruments* 4 (17) (2020), <https://doi.org/10.3390/instruments4020017>.
- [18] T. Suwa, Y. Nabara, Y. Takahashi, Cable behavior during manufacture of a 900-m scale CICC, *IEEE Trans. Appl. Supercond.* 26 (4) (2006), <https://doi.org/10.1109/TASC.2016.2543465>.
- [19] N.C. vanden Eijnden, A. Nijhuis, Y. Ilyin, Axial tensile stress-strain characterization of ITER model coil type Nb3Sn strands in TARSIS, *Supercond. Sci. Technol.* 18 (2005) 1523–1532, <https://doi.org/10.1088/0953-2048/18/11/020>.
- [20] Z.C. Zhang, D.S. Yang, H.S. Zhou, et al., Degradation mechanism of the superconducting performance of a Bi2212 cable under magnetic fields, *Supercond. Sci. Technol.* 35 (2022) 035004, <https://doi.org/10.1088/1361-6668/ac4ad2>.
- [21] Z.C. Zhang, D.S. Yang, M. Yu, et al., The research on the influence mechanism of internal deformation for the performance of Bi-2212, *Supercond. Sci. Technol.* 36 (2023) 115007, <https://doi.org/10.1088/1361-6668/acf73c>.
- [22] Hugues Bajas, Numerical Simulation of the Mechanical Behavior of the ITER Cable-In-Conduit Conductors, Ecole Centrale Paris, 2011. <https://tel.archives-ouvertes.fr/tel-00697000>.
- [23] J.G. Qin, et al., A 3D numerical model study for superconducting cable pattern, *Fusion Eng. Des.* 85 (1) (2010) 109–114, <https://doi.org/10.1016/j.fusengdes.2009.08.001>.
- [24] C. Dai, B. Liu, J.G. Qin, Study on the mechanical properties of NbTi and Nb3Sn superconducting strand, *J. Low Temp. Phys.* 36 (6) (2014), <https://doi.org/10.13380/j.cnki.chin.j.lowtemp.phys.2014.06.013>.
- [25] T.J. Xue, Z.R. Wei, J.G. Qin, et al., Cabling process control of ITER superconductive cable *Electric Wire Cable*, 6 (2015) 4 [in Chinese].
- [26] Y.P. Teng, S.T. Dai, Z.R. Wei, et al., Cabling for the Superconducting Cable of Magnet Coils for ITER, *J. Electr. Eng. Technol.* 28 (4) (2013) 6, <https://doi.org/10.3969/j.issn.1000-6753.2013.04.002> [in Chinese].
- [27] B.H. Wang, An applied engineering method of determining tension by deflection, *Mech. Sci. and Technol. Aerospace Eng.* 1 (1991) 4 [in Chinese].
- [28] I. Samset. Winch and Cable systems[M]. Springer Netherlands, 1985. <https://doi.org/10.1007/978-94-017-3684-8>.